Journal of Applied Polymer Science

WILEY

Applied Polymer SCIENCE

RESEARCH ARTICLE OPEN ACCESS

Simvastatin-Release Photocurable Hydrogel With Microsphere Delivery System for Improved Dental Applications

Erika S. Bronze-Uhle[1] | Isabela S. P. Silva[1] | Ester A. F. Bordini[2] | Vitor T. Stuani[1] | Camila C. S. B. Melo[1] | Priscila T. A. de Toledo[1] | Ligia E. Correa[1] | Daniel Rinaldo[3] | Carlos A. de Souza-Costa[4] | Paulo N. Lisboa-Filho[5] | Diana G. Soares[1]

[1]Department of Operative Dentistry, Endodontics and Dental Materials, Bauru School of Dentistry, São Paulo University – USP, Bauru, Brazil | [2]Department of Dental Materials and Prosthodontics, Ribeirao Preto School of Dentistry, São Paulo University – USP, Ribeirao Preto, Brazil | [3]Department of Chemistry, School of Science, São Paulo State University – UNESP, Bauru, Brazil | [4]Department of Physiology and Pathology, Araraquara School of Dentistry, São Paulo State University – UNESP, Araraquara, Brazil | [5]Department of Physics, School of Science, São Paulo State University – UNESP, Bauru, Brazil

Correspondence: Diana G. Soares (dianasoares@fob.usp.br)

Received: 15 September 2024 | **Revised:** 12 February 2025 | **Accepted:** 19 April 2025

Funding: This work was supported by the Coordenação de Aperfeiçoamento de Pessoal de Nível Superior—Brazil (CAPES)—Finance Code 001 and from the Fundação de Amparo à Pesquisa do Estado de São Paulo (FAPESP)—Grant Numbers 2016/15674-5 and 2022/05888-9.

ABSTRACT

The development of multifunctional injectable biomaterials that serve as frameworks for tissue neo-deposition and promote dentin regeneration through resident dental pulp cells represents an innovative approach in regenerative dentistry. This study presents an injectable system based on a photocrosslinkable hydrogel, functionalized with a drug release system to deliver bioactive doses of the biomineralizing drug simvastatin. Chitosan microspheres (MSCH) loaded with 2%, 5%, or 10% simvastatin (MSCHSV) were prepared and incorporated into gelatin methacryloyl (GelMA) to create a hybrid hydrogel activated by LED light. Characterizations, including Fourier transform infrared (FTIR), scanning electron microscopy (SEM), pore size, porosity, and swelling capacity, confirmed the inclusion of particles and creation of a 3D biomaterial. The inclusion of microspheres did not alter the hydrogel's degradability under enzymatic action. Biostimulation of human dental pulp cells (HDPCs) on the hydrogel was evaluated through cell viability and mineralized matrix assays. Results showed no cytotoxic effects, with significant cell proliferation over time. HDPCs displayed an increase in mineralization nodules when cultured with GelMA functionalized with MSCH containing 2%, 5%, and 10% simvastatin. However, only the 10% concentration resulted in a significant increase. Thus, incorporating chitosan microspheres with 10% simvastatin into GelMA creates a controlled release system with high potential for direct pulp capping.

1 | Introduction

Minimally Invasive Dentistry emphasizes the preservation of dental tissues to maintain the vitality and homeostasis of the dentin-pulp complex. Vital pulp therapy (VPT) aims to preserve this complex even in challenging clinical situations [1, 2]. In cases of exposed pulp tissue with regenerative potential, the goal is to apply a biomaterial that induces the formation of a mineralized barrier by resident pulp cells, thereby sealing the complex and maintaining pulp viability [3]. While alkaline cements like calcium hydroxide and calcium silicate are commonly used for this purpose, they have limitations,

including high solubility, poor sealing, and induction of tissue necrosis and inflammation. Moreover, their application is complicated by the need for proper coverage and contact with the tissue [3, 4].

These challenges have led researchers to explore alternative clinical solutions that facilitate application and enhance repair by resident mesenchymal stem cells without local toxicity. Translating tissue engineering strategies into regenerative dentistry offers a promising approach for developing safe and reliable biomaterials to regenerate the dentin-pulp complex [5–7]. Injectable biomimetic scaffolds are particularly advantageous as they easily adapt to defects, providing a simpler clinical application [8, 9].

One biomaterial gaining significant attention in dentin tissue engineering is methacrylated gelatin hydrogel (GelMA), derived from the modification of gelatin's amine groups with methacrylate groups [10]. GelMA is a protein substance extracted from the collagen of bovine or porcine skin or bone, consisting of denatured and partially hydrolyzed native collagen, primarily type I collagen [11]. Despite being denatured, it retains bioactive collagen sequences, such as arginine-glycine-aspartic acid (RGD) peptides, which promote cell adhesion, as well as matrix metalloproteinase (MMP) target sites, crucial for tissue remodeling [12]. A significant advantage of using GelMA for dentin repair applications is its ability to combine with a photoinitiator activated under visible light, such as Lithium acylphosphinate (LAP), enabling defect-specific injection and in situ photopolymerization using LED devices available in dental offices [13]. Furthermore, the physicochemical and mechanical properties of GelMA can be easily modulated by adjusting the polymer and LAP concentration, as well as the photopolymerization time, optimizing both the material's properties and the tissue response [14, 15].

In the context of dentin tissue engineering, cell homing has been a natural choice, as pulp stem cells would be mobilized towards the scaffold, and the porous architecture would allow cells to infiltrate the scaffold structure [16]. Therefore, the incorporation of bioactive cues is essential to improve chemotaxis, cell recognition, proliferation, and differentiation, thereby promoting mineralized tissue. Our group has focused on strategies based on simvastatin-loaded scaffolds for dentin tissue engineering, due to their potential as chemoattractants for precursor pulp-tissue cells, leading the cells to express an odontoblastic phenotype and deposit a mineralized matrix in vitro [17–19]. A bioactive dosage ranging from 0.1 to 0.01 uM has been selected, and we have already observed that a chitosan scaffold incorporated with simvastatin has been shown to be a highly bioactive biomaterial for dentin tissue engineering. Nevertheless, a bulk scaffold does not seem adequate for application on dental pulp exposure due to the need for biomaterial adaptation, and the incorporation method leads to a burst release within 24 h.

To address this concern, chitosan microspheres encapsulated with simvastatin were developed by Bronze-Uhle et al. (2025) [20], which were able to release bioactive dosages of this drug in a sustained manner. When applied in direct contact with a 3D culture of human dental pulp cells, these microspheres led to increased mineralized matrix deposition by 2.3 to 2.6 times compared to the negative control. Nevertheless, the direct in situ application of microspheres carries the same disadvantage as the cements used in clinical scenarios for direct pulp capping: controlling their application on exposed dental pulp and ensuring complete tissue coverage. Previous studies [21] also suggested that when applied in vivo, microspheres may be eliminated or migrate away from the implantation site [22, 23].

Since the hydrophobic nature of simvastatin impairs its homogeneous distribution in the hydrophilic matrix of hydrogels, leading to rapid drug release and low bioavailability through surrounding tissues [22, 24, 25], and encapsulating simvastatin into microspheres improves its dispersion in hydrophilic biomaterials and creates a sustained delivery system [26–30], in this study, we propose incorporating chitosan-simvastatin microspheres into GelMA to create hybrid superstructures. The potential of hybrid hydrogels based on GelMA and chitosan has been explored in the literature, leveraging the mechanical properties, injectability, in situ photopolymerization, and local stability associated with the surrounding hydrogel, providing a multifunctional platform for mineralized tissue regeneration [31, 32].

2 | Materials and Methods

2.1 | Synthesis and Characterization of Chitosan (MSCH) and Chitosan-Simvastatin (MSCHSV) Microspheres

A chitosan solution (low molecular weight in 2% v:v acetic acid solution; Sigma-Aldrich, St. Louis, MO, USA) was subjected to a water-in-oil emulsion in liquid paraffin (Merck KGaA, Darmstadt, Germany) containing span 80 surfactant (Sigma-Aldrich, St. Louis, MO, USA) at 2000 rpm for 5 min (Polytron homogenizer, Kinematica Littau/Lucerne, Switzerland). To encapsulate simvastatin (Sigma-Aldrich, St. Louis, MO, USA), solutions at 2%, 5%, and 10% (w:w relative to the chitosan mass) were prepared in pure ethanol Sigma-Aldrich, St. Louis, MO, USA and mixed with the chitosan solution (500 rpm, 5 min) prior to emulsification. Then, glutaraldehyde (Exodo Cientifica, Sumare, SP, Brazil) was incorporated at 2000 rpm for 20 min at 37°C to form the crosslinking and microspheres. Afterward, the solutions were incubated for 30 min at room temperature. Microspheres were collected by successive washing in acetone and water followed by centrifugation at 12,000 rpm for 10 min (Z 326 Hermle Labortechnik GmbH, Wehingen, Germany). The remaining water solution was freeze-dried (Alpha 1–2 LD plus, GmbH, Osterode am Harz, Germany) for 48 h. The following microspheres were prepared: MSCH—chitosan microspheres, MSCHSV2%—chitosan microspheres encapsulated with 2% simvastatin, MSCHSV5%—chitosan microspheres encapsulated with 5% simvastatin, and MSCHSV10%—chitosan microspheres encapsulated with 10% simvastatin. Simvastatin concentrations were determined based on the work of Bronze-Uhle et al. (2025) [20], which demonstrated the creation of round microspheres with a smooth surface capable of releasing simvastatin in a sustained manner. These MSCHSV concentrations also featured bioactivity with dental pulp cells in direct contact with them.

In pilot experiments performed by our group, at higher concentrations of simvastatin, no microspheres were formed (data not shown).

2.1.1 | Morphological and Particle Size Characterization

The collected microspheres after lyophilization were analyzed by Scanning Electron Microscopy (SEM) on an EVO LS15 equipment (Carl Zeiss, Jena, Germany) after placement onto carbon adhesive film and coating with a gold jet (Q150R Plus—Rotary Pumped Coater, Quorum, Laughton, England). Particle size was analyzed using Image J software (NIH, Bethesda, MD, USA) immediately after microsphere synthesis. A total of 100 structures were measured in 3 samples for each formulation.

2.2 | Synthesis of Gelatin Methacryloyl (GelMA Precursor)

Type A porcine skin gelatin (Sigma-Aldrich, St. Louis, MO, USA) 10% (w/v) was solubilized in 100 mL of phosphate-buffered saline (PBS; pH 7.4, Gibco, Invitrogen, Carlsbad, CA, USA) at 50°C. After complete dissolution, 8 mL of methacrylic anhydride (Sigma-Aldrich, St. Louis, MO, USA) was slowly added and stirred for 2 h. To stop the reaction, 100 mL of PBS (Gibco, Invitrogen, Carlsbad, CA, USA) at 50°C was added and stirred for 15 min. The solution was dialyzed for 5 days at 40°C in deionized water using a 12–14 kDa dialysis membrane (Spectro/Por molecular porous membrane tubing, MWCO 12–14,000, SpectrumLabs Inc., Rancho Dominguez, CA, USA) to remove the excess of methacrylic acid and any residual monomers. The solution was filtered and frozen at −80°C for 24 h and freeze-dried at −56°C (150×10^{-3} Mbar; Liotop, Liobras, São Carlos, SP, Brazil) for 7 days to generate a porous white foam, which was stored at −20°C.

2.3 | Preparation of GelMA-MSCH and GelMA-MSCHSV Hybrid Structures

Freeze-dried GelMA precursor (15% w/v) was dissolved in sterile PBS 1× (pH 7.4, Gibco, Invitrogen, Carlsbad, CA, USA) containing 0.075% (w/w) of the Lithium phenyl-2,4,6-trimethylbenzoylphosphinate salt as a photoinitiator (LAP, Sigma—Aldrich) at 40°C. The MSCH, MSCHSV2%, MSCHSV5%, and MSCHSV10% were each added in a proportion of 2.5 mg/mL (w/v) to the GelMA solution and homogenized in a vortex at 37°C. This concentration was selected based on a pilot experiment, as higher concentrations of simvastatin resulted in the leachable components of the microspheres being toxic to dental pulp cells (Figure S1). Afterward, 100 μL of plain and hybrid solutions were pipetted into a 96-well plate and exposed to 1200 mW/cm^2 LED light (385–515 nm, Bluephase N, Ivoclar-Vivadent, Buffalo, NY, USA) for 30 s to complete polymerization and formation of the hybrid 3D hydrogel [15]. The following groups were established: GelMA-MSCH, GelMA-MSCHSV2%, GelMA-MSCHSV5%, and GelMA-MSCHSV10%.

2.4 | Physical–Chemical Characterization and Properties of Hybrid Hydrogels

2.4.1 | Spectral Analysis of Chemical Interactions

Fourier transform infrared spectroscopy (FTIR) was performed to determine the synthesis of microspheres, GelMA, and chemical interactions after microsphere incorporation. Before analysis, the hydrogel samples ($n = 3$) were freeze-dried for 24 h at −56°C (150×10^{-3} Mbar; FreeZone, Labconco Corporation, Kansas City, MO, USA). The spectra were obtained in attenuated total reflection mode (ATR mode) using an IR PRESTIGE-21 equipment (Shimadzu, Kyoto, Japan) in the range of 400 to 4000 cm^{-1} at 4 cm^{-1} resolution (32 scans).

2.4.2 | Morphology Assessment

The surface morphology of the 3D hydrogels was evaluated using SEM (EVO LS15, Carl Zeiss, Jena, Germany). Samples were prepared, stored for 14 days at −20°C, and lyophilized for 24 h at −56°C (150×10^{-3} Mbar; FreeZone, Labconco Corporation, Kansas City, MO, USA). The different materials were fixed to an electrical adhesive film (carbon) and coated with a gold jet (Q150R Plus—Rotary Pumped Coater, Quorum, Laughton, England). Pore size and porosity were evaluated under SEM employing Image J software, using 6 images per sample ($n = 3$) (NIH, Bethesda, MD, USA). Microsphere particle size was analyzed using ImageJ software (NIH, Bethesda, MD, USA). A total of 40 particles from three samples of each formulation were measured. Agglomerates were highlighted in blue using Pixelmator Pro 2 software (Vilnius, Lithuania).

2.4.3 | Swelling Properties

The swelling capacity of the hydrogels was evaluated immediately after polymerization in a 96-well plate (6 mm in diameter × 2 mm in thickness, $n = 5$). The hydrogels were incubated in PBS (Gibco, Invitrogen, Carlsbad, CA, USA) at 37°C for 24 h to reach the equilibrium swelling state. After the period, they were dried on paper (Kimberly-Clark, Irving, TX, USA) and weighed on an analytical balance to obtain wet weights (Ww). They were then lyophilized (24 h at −56°C, 150×10^{-3} Mbar; Liotop), and their dry weight (Wd) and swollen weight (Ws) were recorded. The swelling ratio (%) was calculated by [(Ws—Wd)/Wd] × 100% [33].

2.4.4 | Enzymatic Degradability

For degradation profiles, specimens freshly prepared by polymerization (6 mm in diameter × 2 mm in thickness, $n = 7$) were placed in a 48-well plate containing 1 mL of sterile PBS 1× (Gibco, Invitrogen, Carlsbad, CA, USA) for 24 h to achieve swelling balance (Wt0). Then, the type I collagenase enzyme (Sigma-Aldrich) was added at a proportion of 1 U/mL in PBS and kept at 37°C. Freshly prepared solution containing collagenase was changed every 72 h to maintain enzymatic activity [16]. At specific time intervals (1, 3, 7, and 14 days), samples were removed from the collagenase solution, washed with

deionized water (2x), and dried on paper (Kimberly-Clark, Irving, TX, USA). Weight (Wt) was determined on an analytical balance (BelEngineerin, Monza, MI, Italy). The degradation rate was calculated according to the equation: [(Wt/Wt0) × 100%] [33, 34].

2.4.5 | Simvastatin Release

To observe the simvastatin release through microspheres into the hydrogel, samples measuring 16 mm in diameter and 2 mm in thickness were prepared in 24-well plates and incubated with 1 U/mL type I collagenase solution in ultra-pure water (Thermo Fisher Scientific) and kept at 37°C. Then, the supernatant was collected after 1, 3, 5, and 7 days. The samples were lyophilized (Alpha 1–2 LD plus, Martin Christ GmbH, Osterode am Harz, Germany), resuspended in 500 μL ethanol, and filtered (0.45 mm, Kasvi, São José dos Pinhais, PR, Brazil) for absorbance measurement at 230 nm (Synergy H1, BioTek, Winooski, VT, USA). Cumulative release was calculated using a standard curve [26], and data was normalized by scaffold volume (mm^3).

2.4.6 | Injectability and Volume Measurements

The injectability of the hydrogels was assessed by extruding them through a 3 mL syringe with a 22-gauge needle. The assay was performed using a piston-based extrusion bioprinter (TissueStart 3D Bioprinter, TissueLabs Sagl, Switzerland) in extrude mode [15]. A pressure of 101.8 kPa was applied, and the extruded mass was measured ($n = 6$). Given that GelMA undergoes thermogelation, the assay was standardized at room temperature (20°C). For volume measurements, 2 mL of hydrogels was placed in 1.1 cm radius (r) cylindrical flasks and subjected to photopolymerization. The height (h) of the hydrogels was measured at three points, and volume was calculated using the formula $v = \pi r^2.h$ ($n = 6$). Representative images of GelMA viscosity at 37°C, 20°C, and after photoactivation were captured with a digital camera, as well as during the injectability assay.

2.5 | In Vitro Biological Evaluation

2.5.1 | Cell Culture on Hydrogels

The primary culture of human dental pulp cells (HDPCs) was cultivated with complete α-MEM (alpha Minimum Essential Medium, supplemented with 10% fetal bovine serum [FBS], L-glutamine, and 1% penicillin–streptomycin, 1% anti-anti; Gibco by Thermo Fisher Scientific, Waltham, MA, USA) and maintained at 37°C and 5% CO_2 until confluence. The HDPCs used for this experiment were obtained by the enzymatic disaggregation method from sound third molars collected from four young patients (18–20 years) after approval by the ethics committee, and each patient signed a consent form (Human Research Ethics Committee—Bauru School of Dentistry, University of São Paulo—USP—CAAE protocol # 53489421.9.0000.5417). The cells were obtained according to the protocols established by Soares et al. (2018) [17], and the pool of cells between passages 4–7 was used.

A volume of 100 μL of sterile hydrogels was applied to 96-well plates (Kasvi), followed by photopolymerization for 30 s, as previously described, creating samples with 6 mm in diameter x 2 mm in thickness. Then, the cells were trypsinized, counted, and suspended in the culture medium at a concentration of 1×10^4 cells/100 μL to be added to the hydrogels. This set was incubated at 37°C and 5% CO_2, with the culture medium being changed every 48 h.

2.5.2 | Live/Dead Assay

The viability of HDPCs was qualitatively evaluated in hydrogels using the Live/Dead viability/cytotoxicity kit (Invitrogen, Thermo Fisher Scientific, Eugene, OR, USA) for 1, 3, 7, and 14 days ($n = 3$). Calcein AM and Ethyl Homodimer-(Live/Dead cell viability/cytotoxicity kit; Invitrogen, Waltham, MA, USA) in the ratio of 0.25:1.0:1000 (v/v/v) respectively, for 2 min, were used as markers of live (green) and dead (red) cells, respectively. Fluorescence microscopy (EVOS Cell Imaging Systems, Life Technologies, Carlsbad, CA, USA) was used to evaluate the images on the surface of the GelMA derivatives.

2.5.3 | Cell Viability

The quantitative assessment of cell viability, expressed by cellular metabolic activity, was performed using the Alamar Blue assay (Life Technologies, Carlsbad, CA, USA) at 1, 3, 7, and 14 days ($n = 6$). For the analyses, 3D hydrogels were incubated for 3 h at 37°C and 5% CO_2, with a 10% solution (v/v) Alamar Blue in an α-MEM solution (without FBS). Afterward, the fluorescence of the solution was measured at 540 nm excitation and 590 nm emission in a microplate reader (Synergy H1, Biotek, Winooski, VT, USA).

2.5.4 | Alkaline Phosphatase (ALP) Activity

ALP activity was measured after 14 days of cell/hydrogel culture in osteogenic medium (α-MEM with 50 μg/mL ascorbic acid and 10 mM β-glycerophosphate). The Alkaline Phosphatase—Endpoint Assay kit (Labtest, Lagoa Santa, MG, Brazil) was used. Samples were incubated in 0.1% sodium lauryl sulfate solution, then centrifuged, and the supernatant was mixed with thymolphthalein monophosphate substrate and incubated at 37°C for 15 min. After adding the color reagent, absorbance was measured at 590 nm. Total protein was quantified using Lowry Reagent (Sigma-Aldrich), and absorbance was read at 655 nm (Synergy H1, Biotek). ALP activity was normalized to total protein, and data was converted to percentage based on the negative control group.

2.5.5 | Collagen Expression

Extracellular soluble collagen expression ($n = 6$) was assessed using a fluorescence assay with the Collagen Assay Kit MAK322 (Sigma-Aldrich). Constructs were cultured in osteogenic medium for 7 days, with medium collected every 72 h. Samples underwent enzymatic digestion, followed by

the reaction of N-terminal glycine peptides with a fluorescent probe. Quantification was performed by measuring fluorescence (375 nm excitation; 465 nm emission; Synergy H1, Biotek), using a standard curve to determine collagen concentration, and data was converted to the percentage of the negative control.

2.5.6 | Mineralized Matrix Deposition

The mineralization nodules deposition was evaluated after 21 days ($n = 10$) in an osteogenic medium. The samples were fixed with 70% ethanol for 1 h at 4°C and washed with deionized water (1×). Subsequently, they were incubated in alizarin red solution (40 mM, pH 4.2; Sigma Chemical, Sigma-Aldrich) for 15 min and washed with deionized water (3×). The stained hydrogels were photographed with a digital camera, and the stain was dissolved in 200 μL of 10% cetylpyridine chloride solution (Sigma-Aldrich, St. Louis, MO, USA). Quantitative analysis was obtained through absorbance in a microplate reader (Synergy H1, BioTek, Winooski, VT, USA) at 570 nm. Hydrogels with no cells were used as a blank for background control.

2.6 | Statistical Analysis

Three independent experiments were performed for quantitative assays. Data was compiled and analyzed by one or two-way ANOVA, complemented by the Tukey test, using GraphPad 10.2.1. software. Significant differences were considered at 5%.

3 | Results and Discussion

3.1 | Synthesis and Characterization of Microspheres and Hybrid Structures

SEM images of microspheres and hydrogels, along with bar graphs of porosity degree, pore size, and particle diameter measurements on hydrogels are depicted in Figure 1. The MSCH and MSCHSV2%, MSCHSV5%, and MSCHSV10%, processed by the emulsion-crosslinking method, were round and had mean sizes of 1.7 ± 0.2 μm; 1.05 ± 0.15 μm; 1.3 ± 0.2 μm; and 0.85 ± 0.3 μm, respectively (Figure 1a). The characterization of microspheres was previously reported by Bronze-Uhle et al. (2025) [20]. These microspheres presented a round and smooth surface with a percentage yield above 88% and drug encapsulation efficiency above 84%. The presence of simvastatin was confirmed by FTIR, and a sustained release proportional to simvastatin concentration was observed throughout 30 days.

The morphological properties of hydrogels are illustrated in Figure 1b. SEM images of GelMA hydrogels confirm the macroporous morphology. An irregular porous architecture was observed for the formulations incorporated with microspheres tested in this stage. The microspheres were present throughout GelMA with a tendency to form agglomerates. Those seemed to be higher as simvastatin concentration on microspheres was increased. These agglomerates can be observed on high magnification SEM images of Figure 1b, highlighted in blue. Figure 1c presents a dispersion graph encompassing the measurement of microspheres on GelMA. It is possible to note that all groups present variations in the diameter of particles measured, with GelMA-MSCHSV10% featuring aggregates with higher diameters. Nevertheless, no significant differences were observed among groups when mean values were compared. The overall porosity (Figure 1d) significantly increased with the inclusion of MSCHSV compared to plain GelMA regardless of simvastatin concentration. Statistically similar pore sizes were obtained for the hydrogels GelMA (30.0 ± 5.4), GelMA-MSCH (24.2 ± 2.2), GelMA-MSCHSV2% (26.4 ± 2.4), and GelM-MSCHSV5% (30.6 ± 2.7). Nevertheless, GelMA-MSCHSV10% featured significantly higher pore size (53.2 ± 11.8) than the other groups (Figure 1e).

The morphology, pore size, and porosity of biomaterials are important factors to evaluate in the synthesis process of novel biomaterials, as they influence mechanical properties and cellular response. Pore architecture, interconnectivity, and size are crucial in the regeneration processes, allowing local cell adhesion, proliferation, and angiogenesis, as they are closely associated with oxygen diffusion, nutrient transport, and cellular vascularization [7, 16]. The introduction of microspheres changes the proportions of covalent and physical bonds in the 3D matrix. Physical particle-polymer bonds between hydrophilic groups originating from chitosan and GelMA increase crosslinking, which may affect pore size [35, 36]. In the presence of a high dosage of simvastatin in GelMA-MSCHSV10%, the energy balance of the interactions involved probably increased the polymer-particle distance, thus increasing the pore size [35, 37]. In addition, Moghimikheirabadi et al. (2021) [35] report that the miscibility and good dispersion of nanoparticles within the polymer matrix are often associated with the effective nanoparticle-polymer attraction strength. Furthermore, hydrophobic modifications affect the microstructure of the hydrogel, as they lead to the formation of larger polymeric crowns around particles, increasing the hydrodynamic radius and the polymer-particle distance [38, 39]. Therefore, the higher simvastatin concentration in MSCHSV10% may have provoked higher aggregates, leading to hydrogel structure expansion due to the hydrophobic nature of those aggregates.

The FTIR spectrum of hydrogels is presented in Figure 2. GelMA exhibits characteristic absorption bands in its structure [40–42]. The band at 3290 cm^{-1} refers to the stretching of —OH groups of hydroxyproline present in the structure. The other absorption bands are relative to 3200–3400 cm^{-1} (N—H stretching of peptide bonds), 2945 and 2934 cm^{-1} (symmetric and asymmetric stretching of amides and C—H groups of alkyl chains, respectively), 1650 cm^{-1} (C═O stretching of amide I), 1639 and 1539 cm^{-1} (C═O stretching of amide I and angular N—H deformations of amide II), 1500–1570 cm^{-1} (angular deformations of —N—H groups of amide II), and 1240 cm^{-1} (angular deformations of N—H groups and C—N stretching of amide III). Characteristic absorption bands of amides are observed due to the presence of methacryloyl groups [42]. The FTIR analyses of GelMA-MSCH and GelMA-MSCHSV (2%, 5%, and 10%) demonstrate changes in intensity and displacement that corroborate the inclusion of the spheres in the hydrogel. The increase in bands in the 2911–2854 cm^{-1} and 1070–1030 cm^{-1} regions indicates the

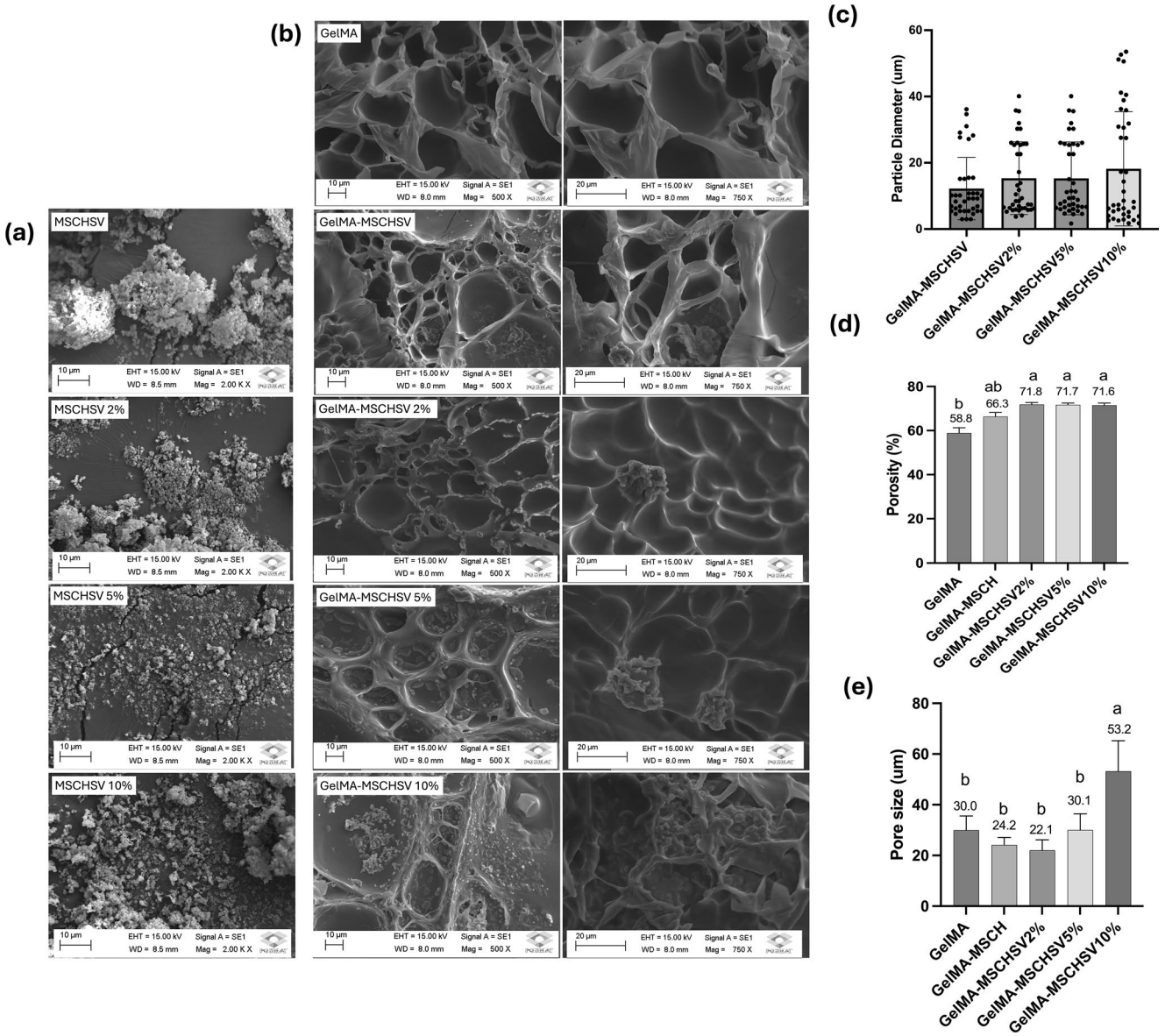

FIGURE 1 | (a) SEM images (2.00 K X magnification) of microspheres. (b) SEM images (500 X and 750 X magnification) of hydrogels. Note microspheres agglomerates in blue. (c) Dispersion graph of particle diameter measurement on SEM images (500 X). Representative bar graph of porosity (d), and pore size (e) for hydrogels. Numbers are mean values. Different letters indicate significant differences among groups (One-way ANOVA; Tukey's test. $p < 0.05$).

insertion of MSCH and MSCHSV into the hydrogel structure. Subtle changes in intensity and displacement in the regions 3400–3300 cm^{-1} and 1650–1370 cm^{-1} indicate interactions (electrostatic and hydrogen bonds) between functional groups on the surface of the chitosan microparticle with functional groups in the GelMA structural network [40, 43].

The FTIR performed for microspheres confirmed the incorporation of simvastatin for those formulations, as previously demonstrated by Bronze-Uhle et al. (2025) [20]. MSCH and MSCHSV present absorption bands in the regions of 3500–3100 cm^{-1} (—OH and —NH stretches), 2922 and 2854 cm^{-1} (asymmetric and symmetric —C—H stretches), 1650 cm^{-1} (relative to the C═O stretching of amide groups I), 1638 and 1560 cm^{-1} (angular vibrations of —NH2) and 1312 cm^{-1} (relative to the C—N stretching bands), 1452 and 1303 cm^{-1} (relative to the deformations of —CH and —OH), 1373 cm^{-1} (related to angular deformations of —C—H groups), 1180–900 cm^{-1} (related to symmetric and asymmetric stretching vibrations of —C—O groups [C—O—C]), and 893 cm^{-1} (characteristic of the saccharide structure of chitosan). Bands at 1644 cm^{-1} refer to stretching vibrations of —C═N— groups, and bands at 1558 cm^{-1} refer to amides and ethylenic bonds (—C═C—), both arising from crosslinking with glutaraldehyde and $-NH_2$ groups of chitosan to form the microsphere. The characteristic band of the aldehyde group (—HC═O) appears at 1714 cm^{-1}, indicating the insertion of glutaraldehyde and chain elongation due to intermolecular crosslinking related to the formation of chitosan microspheres. The insertion of simvastatin is confirmed by changes in the amino groups ($-NH_2$) and/or hydroxyls (—OH) and aldehydes (CH═O) present in the microspheres. The small absorption band at 1708 cm^{-1} is related to the C═O groups of simvastatin [44–46].

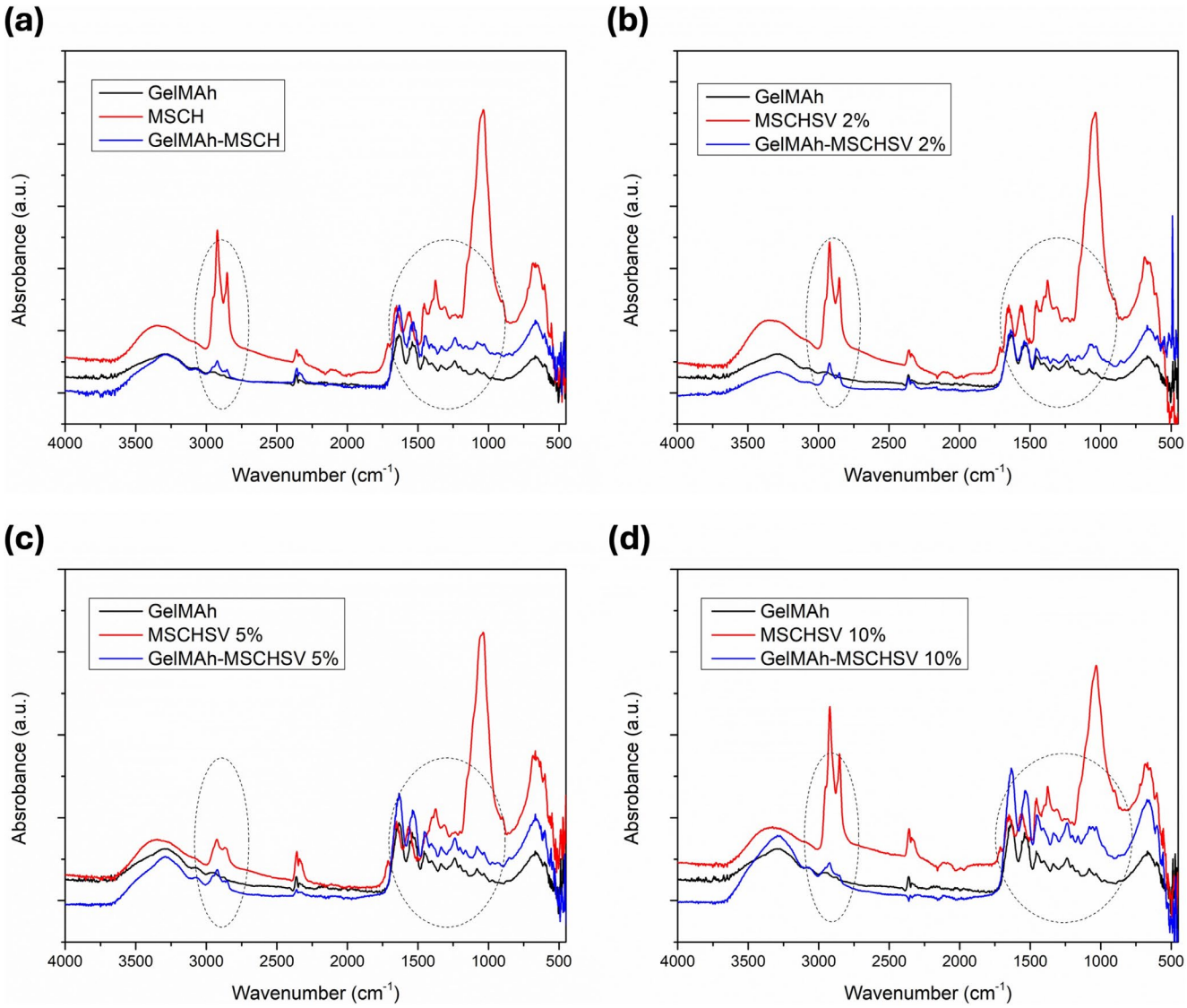

FIGURE 2 | FTIR spectra for (a) GelMA, MSCH, and GelMA-MSCH; (b) GelMA, MSCHSV2%, and GelMA-MSCHSV2%; (c) GelMA, MSCHSV5%, and GelMA-MSCHSV5%; (d) GelMA, MSCHSV10%, and GelMA-MSCHSV10%. [Color figure can be viewed at wileyonlinelibrary.com]

3.2 | Physical Characterizations and Drug Release Assay

Figure 3a shows the swelling ratio for formulated hydrogels. The swelling rate slightly increased with the inclusion of microspheres, with significant differences being observed between the GelMA-MSCHSV groups in comparison to GelMA. However, no significant differences were observed among the groups of GelMA incorporated with microspheres. The higher swelling of GelMA in the presence of chitosan microspheres may be associated with the hydrophilicity arising from NH_2 and OH groups in the chitosan polymer chains [47]. However, the lack of a significant difference between the GelMA-MSCHSV2%, GelMA-MSCHSV5%, and GelMA-MSCHSV10% groups indicates that the presence of hydrophobic simvastatin was not enough to change the extension properties of the polymer chains [40, 48]. The expansion of the hydrophilic polymeric network occurred due to the absorption of the surrounding medium, affecting rigidity, surface mobility, and solute diffusion. For example, greater absorptive capacity can decrease mechanical properties but could facilitate nutrient transport and oxygen diffusion to cells and stimulate cell migration and proliferation [33, 49].

The in vitro degradation rate of the hydrogels in the presence of collagenase is shown in Figure 3b. The results demonstrate that the degradation rate of hydrogels was not significantly different among tested formulations. The biomaterials had a mass loss of 38.3% ± 3.1% after 3 days, and at 7 days, all groups had a very small mass that could not be measured. Therefore, the incorporation of chitosan microspheres into the hydrogel matrix before photopolymerization did not alter the chemical degradability sites associated with collagenase [34]. Numerous articles reported in the literature found degradation results ranging from hours to days, depending on the physicochemical properties of GelMA hydrogels; therefore, controlling degradation is an important factor in the synthesis of 3D hydrogels to support tissue repair and regeneration [40, 50, 51]. In addition to the influence of the type and number of cross-links, degradability is related to the amino acid sequences in the gelatin structure, such as amino groups (from lysine and hydroxylysine residues), hydroxyls (from

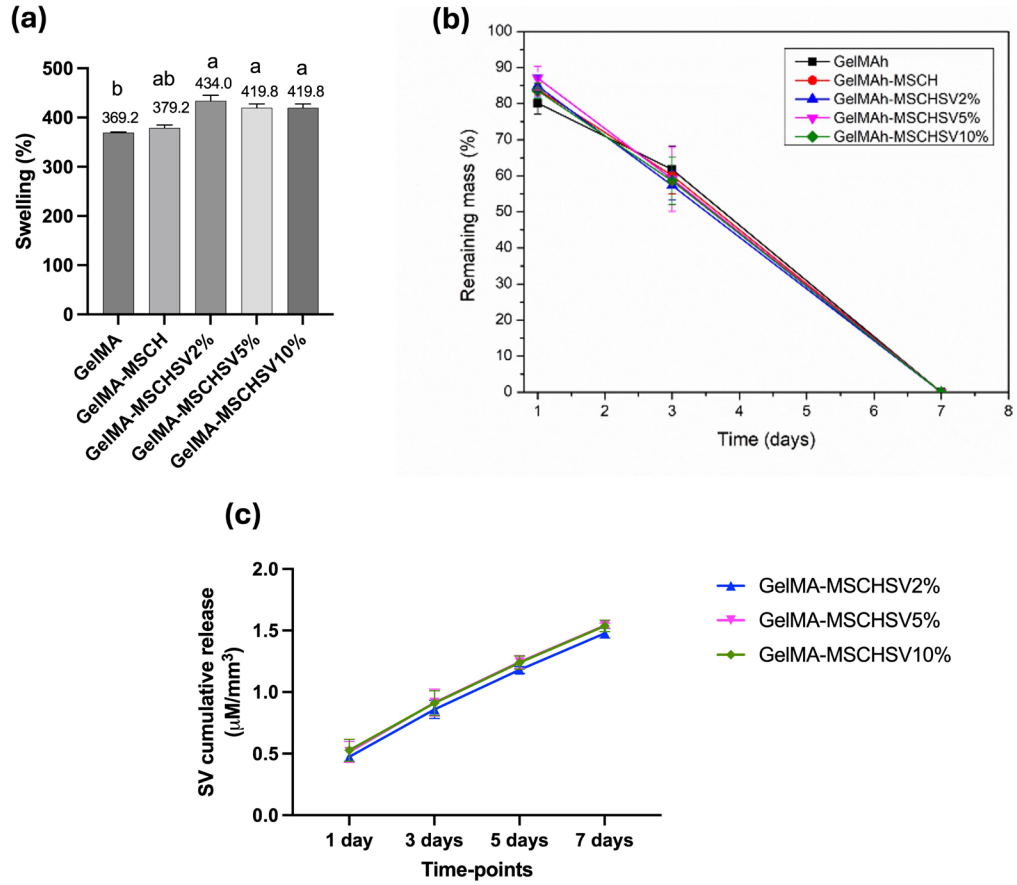

FIGURE 3 | (a) Swelling ratio, (b) Enzymatic degradability of the hydrogels: GelMA, GelMA-MSCH, GelMA-MSCHSV2%, GelMA-MSCHSV5%, and GelMA-MSCHSV10%, and (c) Simvastatin cumulative release from GelMA hydrogel with collagenase. Different letters indicate significant differences among groups (One-way ANOVA; Tukey's test. $p < 0.05$. $n = 6$). [Color figure can be viewed at wileyonlinelibrary.com]

threonine, serine, and hydroxyproline residues), and carboxylic acids (from aspartic acid and glutamic acid residues) [52]. The chemical structure of GelMA contains natural degradation sites for collagenases and metalloproteinases in the extracellular matrix that can be altered in the synthetic process, especially with the inclusion of particles [53–55].

The drug release was also analyzed under enzymatic challenge (Figure 3c) to observe the presence of released simvastatin through GelMA structure from microspheres, such as proposed by Miyazawa et al. (2015) [53]. Simvastatin release in a cumulative pattern was detected throughout the 7 days of analysis, which agrees with degradability studies in the same conditions. As shown in Figure 3c, the hybrid hydrogels GelMA-MSCHSV2%, GelMA-MSCHSV5%, and GelMA-MSCHSV10% presented similar simvastatin release results in the range of 0.45–1.3 μmolar/mm^3, demonstrating the release of the drug in the hydrogel matrix 3D, within the bioactive dose ranges [17, 56–59]. These results confirm those reported by Bronze-Uhle et al. (2025), which demonstrated sustained release of simvastatin from chitosan microspheres and show that the release continues throughout the GelMA structure. A similar result was found by Miyazawa et al. (2015) [30]. A controlled release system for simvastatin was developed by creating gelatin micelles grafted with L-lactic acid oligomers (LAo) to allow simvastatin water solubilization. This system was incorporated into gelatin hydrogel, followed by chemical crosslinking. A sustained release was observed for up to 7 days, followed by burst release, coinciding with hydrogel degradation under enzymatic challenge.

The injectability of the proposed formulations was confirmed, as all hydrogels were injectable through a 22G syringe, as shown in Figure 4a,b. Previous studies with GelMA indicated that this hydrogel is injectable at room temperature (20°C to 22°C), as it achieves a more favorable rheological characteristic for controlled injection [15]. In the presence of MSCHSV, hydrogel flow slightly increased, leading to a higher mass being injected through the syringe. The low viscosity of GelMA incorporated with MSCHSV can also be observed in the images of Figure 4c, in comparison to plain GelMA and GelMA-MSCH. This enhanced injectability can be correlated with swelling results and may be due to the increased hydrophilicity of GelMA in the presence of chitosan. However, this low viscosity may reduce the mechanical characteristics of GelMA. Nevertheless, our results show a similar degree of degradability under challenging conditions, indicating that, despite the viscosity change, GelMA incorporated with MSCHSV does not significantly alter its physicochemical properties.

The volume of hydrogels following photopolymerization is shown in Figure 4c. A significant increase in hydrogel volume was observed for compositions containing microspheres, with the greatest increase seen in the presence of simvastatin. The GelMA-MSCHSV10% formulation exhibited the highest

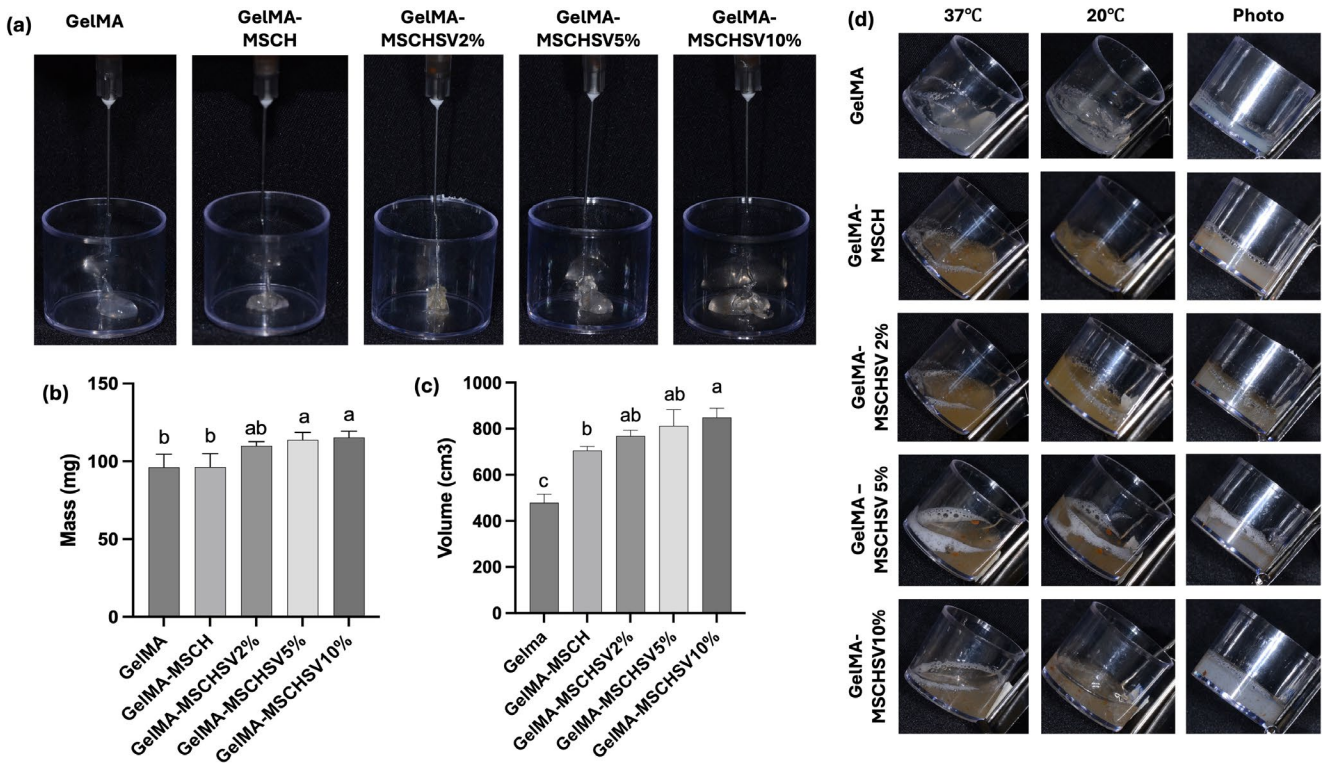

FIGURE 4 | Hydrogel Injectability and volume measurements. (a) Representative images of hydrogels being extruded through a 22 gauge syringe. (b) Mass of extruded hydrogel. (c) Hydrogels volume after photopolymerization. (d) Representative images of hydrogels viscosity at different temperatures and following photopolymerization. Different letters indicate significant differences among groups (One-way ANOVA; Tukey's test. $p < 0.05$. $n = 6$). [Color figure can be viewed at wileyonlinelibrary.com]

volume. The images in Figure 4d illustrate the differences in hydrogel volume and viscosity among the formulations at various temperatures. GelMA undergoes thermogelation due to the presence of gelatin in its composition, meaning its viscosity decreases at higher temperatures. After photopolymerization, all formulations reached a stable form, with higher volumes observed in those containing microspheres.

3.3 | In Vitro Biological Evaluation

Cell viability and proliferation were assessed to evaluate the cytocompatibility of the formulated hydrogels. As shown in Figure 5a, live HDPCs were observed within the hydrogel structures across all compositions. The number of cells within the hydrogels increased over time, with cells covering nearly the entire hydrogel structure by day 14. These findings were further supported by the alamar blue assay data (Figure 5b), which measures cell metabolism and indirectly reflects cell viability and proliferation over time. No significant differences in cell viability were observed among the groups at any of the time points. However, a significant increase in cell viability was observed over time when comparing different time points. The only exception was between the 3 and 7-day time points, where no significant differences were found.

The cell viability results indicate that the hydrogels were cytocompatible, with a high number of live cells observed at all time points. Therefore, it can be concluded that incorporating MSCHSV at concentrations of 2%, 5%, or 10% did not induce cytotoxic effects on HDPCs due to the release of low-dose simvastatin, which has previously been shown to be cytocompatible with dental pulp cells [17, 29, 60, 61]. Previous studies have demonstrated that the effects of simvastatin are concentration-dependent. Concentrations exceeding 5 μM have been shown to negatively affect cell viability. At higher concentrations, simvastatin exhibits anti-proliferative, pro-apoptotic, anti-angiogenic, and anti-invasive properties, and has been widely studied for its ability to inhibit cancer cell proliferation/viability. These effects are directly related to the inhibition of the mevalonate pathway. However, at these higher dosages, a reduction in cell viability has been observed in normal cells, with no bioactive effects reported. Therefore, determining the optimal simvastatin dosage for mineralized tissue regeneration is crucial, and the release pattern of biomaterials should be designed to avoid a burst release of toxic concentrations [62, 63].

The odontoblastic differentiation capacity of HDPCs in vitro was evaluated by evaluating the expression of specific biomarkers. As shown in Figure 6, all biomarkers were positively modulated by GelMA in the presence of simvastatin-loaded microspheres. For both collagen expression and ALP activity, biostimulation showed a trend of being proportional to the simvastatin concentration in the microspheres, with MSCHSV10% exhibiting the highest expressions. However, no significant differences were observed between GelMA-MSCHSV10% and GelMA-MSCHSV5%. The deposition of the mineralized matrix was significantly increased when HDPCs were cultured with GelMA functionalized with MSCHSV2% (59.6%), MSCHSV5%

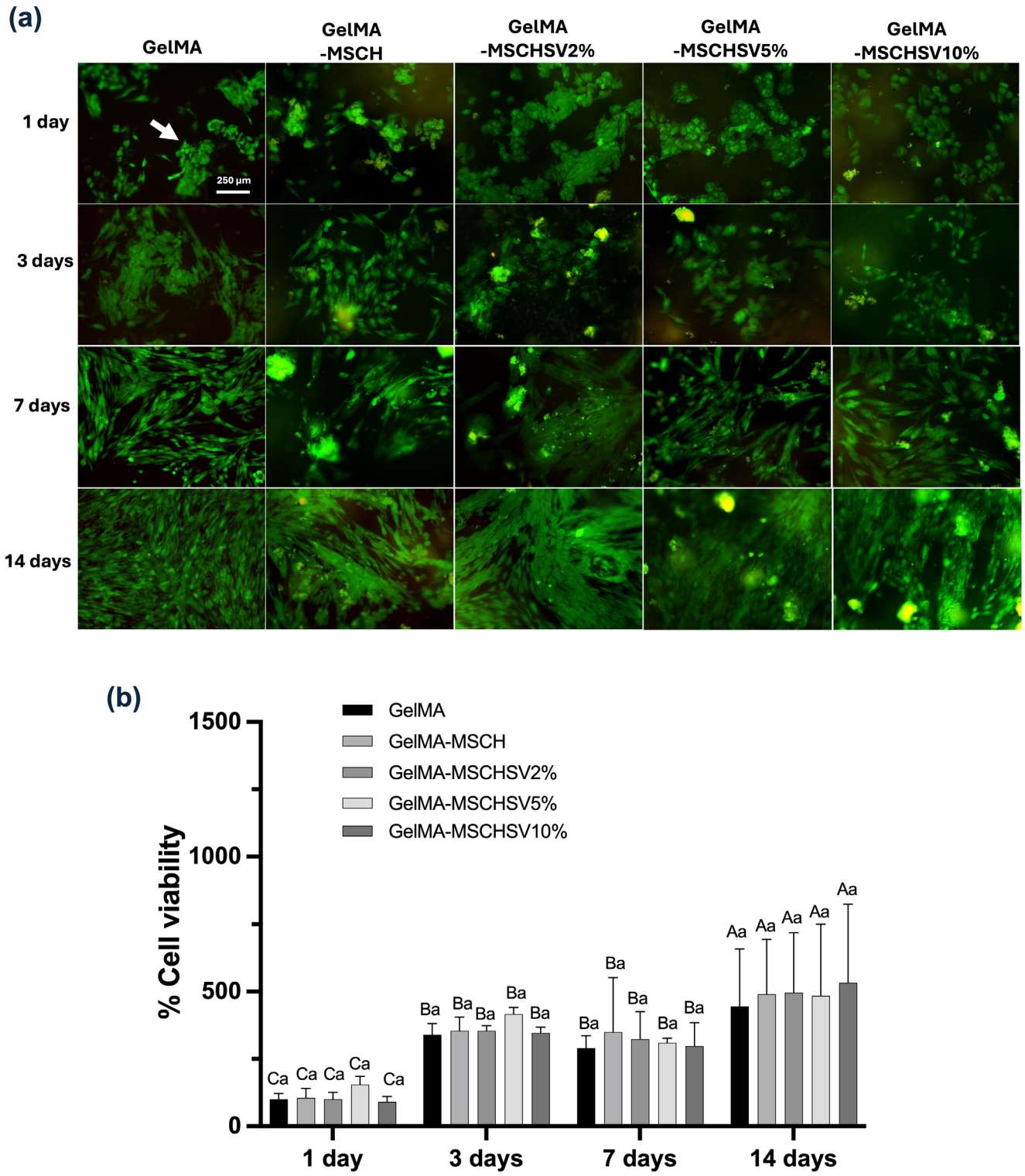

FIGURE 5 | (a) Fluorescence images of the live/dead assay for GelMA, GelMA-MSCH, GelMA-MSCH2%, GelMA-MSCH5%, and GelMA-MSCH10% at periods of 1, 3, 7, and 14 days. Green (live cells) and red (dead cells) staining. (b) Quantitative cell viability using the Alamar Blue metabolic assay (1, 3, 7, and 14 days). Bar graph of mean values of cell metabolism. Capital letters allow comparisons between time points for each group; lowercase letters allow comparisons among groups in each time point. Different letters indicate statistically significant differences (Two-way ANOVA with repeated measures/Tukey. $p < 0.05$. $n = 6$). [Color figure can be viewed at wileyonlinelibrary.com]

(54.4%), and MSCHSV10% (68.2%), compared to plain GelMA. Nonetheless, only GelMA-MSCHSV10% showed a significant increase in comparison to GelMA-MSCH. The increase in red staining (indicating a calcium-rich matrix) in Figure 6d illustrates the presence of MSCHSV in the hydrogels. It is important to note that the hydrogel itself also stains, even in the absence of cells, and was used as the background for the quantitative calculations in Figure 6c.

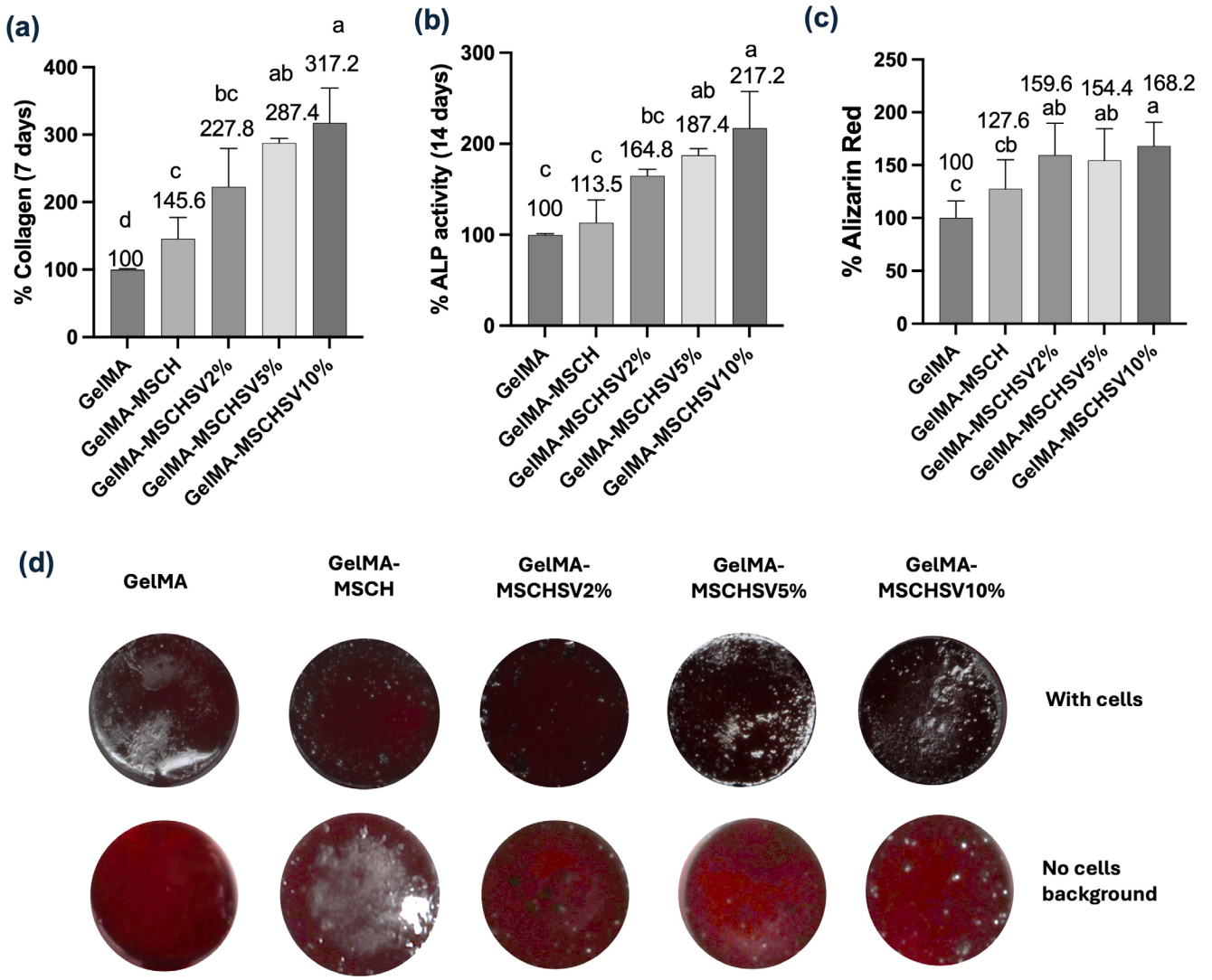

FIGURE 6 | Bar graph of mean values of (a) collagen quantification (7 days), (b) ALP activity (14 days), and (c) alizarin red assay (21 days). Different letters indicate statistically significant differences (One-way ANOVA/Tukey. $p < 0.05$. $n = 6$). (d) Images of calcium nodules stained with alizarin red at 21 days, acquired by digital camera, in the presence and absence of cells (background). [Color figure can be viewed at wileyonlinelibrary.com]

The positive effect on inducing collagen, ALP activity, and calcium-rich extracellular matrix by HDPCs observed in the present investigation has been associated with simvastatin diffusion through the cell membrane and activation of traditional pathways, such as ERK1/2, Smad 1, and BMP-2 pathways, in a mechanism that seems to be independent of the mevalonate pathway, leading to upregulation of BMP-2 and dentin sialophosphoprotein (DSPP), which in turn induce an odontoblastic phenotype [18, 64]. This result corroborates those of Bronze-Uhle et al. (2025) [20], in which the 2%, 5%, and 10% MSCHSV in direct contact with a 3D culture of HDPCs lead to a significant increase in mineralized matrix deposition, demonstrating that the concentration of released simvastatin was within the bioactive range.

A number of in vitro and in vivo studies have shown that 3D biomaterials associated with simvastatin promote bone tissue regeneration [65–68]. In these studies, the authors demonstrated that the effects of simvastatin on regeneration processes are dose dependent. Although the biomineralizing effect of simvastatin was observed when low doses of this drug (0.01 to 1 μM) were continuously used for a specific treatment [17]. In a previous study from our group, bulk scaffolds capable of releasing around 0.1 μM simvastatin had significantly increased bioactive potential on HDPCs. Using a realistic in vitro model of dental pulp exposure, the authors showed that this low amount of simvastatin released from the scaffolds induced the migration of HDPCs from a 3D culture into the permeable biomaterial [17]. Migrating cells expressed an odontogenic phenotype that was upregulated by simvastatin [18]. The positive effect of those simvastatin-enriched scaffolds was confirmed by a cell-free system in calvaria defects created in rats. In the presence of simvastatin, bone regeneration occurred faster and more intensely. Nevertheless, the previously developed system did not sustain the release of simvastatin. Conversely, simvastatin experienced a burst effect within 4 h and was completely released in the first 24 h [18].

Other researchers have attempted to create a direct pulp capping cement by simply mixing simvastatin at a high dosage in ceramic-based cements. The results found on human premolars and rat molars were similar, with a slightly higher rate of chronic inflammation and no significant differences in dentin bridge

deposition compared to the control (plain ceramic cement) [69, 70]. These results may be a consequence of the burst release of simvastatin at high concentration, with no bioactive potential. On the other hand, when biomaterials able to promote a more controlled simvastatin release at lower dosages were tested, an improved dentin bridge deposition was achieved in canine teeth (74,75). The controlled release system for simvastatin developed in a gelatin hydrogel [30] positively influenced alkaline phosphatase (ALP) activity, calcium deposition, and bone morphogenic protein-2 expression by human dental pulp stem cells in vitro and led to ectopic calcium deposition and dentin sialoprotein expression after subcutaneous implantation into mice.

Based on the discussion above, the effective use of simvastatin in tissue engineering for promoting mineralized tissue formation likely requires a system that ensures local, sustained release at bioactive dosages. The hydrogel formulated in this study represents a significant advancement in the development of biomaterials suitable for clinical applications in exposed dental pulp treatments. This hybrid system enables in situ photopolymerization, creating a cytocompatible network capable of releasing bioactive doses of simvastatin. However, there are several limitations to this study that should be addressed in future work, including testing additional GelMA concentrations and incorporating a higher quantity of microspheres into the hydrogel to enhance the biomineralization effect. Moreover, in vivo studies are essential to validate the bioactive potential of these formulations in promoting mineralized tissue deposition, with the goal of achieving results comparable to or exceeding those of currently used biomaterials in clinical practice.

4 | Conclusions

The incorporation of simvastatin-loaded chitosan microspheres into the GelMA hydrogel resulted in minimal changes to chemical bonds and interactions between the polymer and particles, without affecting swelling or degradability, and preserving injectability. This system enabled the controlled release of bioactive doses of simvastatin throughout the hydrogel, creating a cytocompatible 3D network capable of promoting the deposition of a mineralized extracellular matrix. Overall, the GelMA-MSCHSV10% formulation exhibited the highest bioactivity and mineralization effects, suggesting its potential for further development as an injectable system for direct pulp capping procedures.

Author Contributions

Erika S. Bronze-Uhle: conceptualization (lead), data curation (lead), investigation (lead), methodology (lead), writing – original draft (lead). **Isabela S. P. Silva:** conceptualization (equal), methodology (equal), validation (lead). **Ester A. F. Bordini:** data curation (supporting), investigation (equal), methodology (equal), supervision (supporting). **Vitor T. Stuani:** conceptualization (equal), data curation (equal), formal analysis (supporting), investigation (supporting), methodology (supporting), writing – original draft (equal), writing – review and editing (equal). **Camila C. S. B. Melo:** investigation (equal), methodology (equal). **Priscila T. A. de Toledo:** methodology (equal), writing – review and editing (lead). **Ligia E. Correa:** formal analysis (equal), methodology (equal), writing – review and editing (lead). **Daniel Rinaldo:** conceptualization (lead), data curation (equal), formal analysis (equal), investigation (equal), methodology (equal), validation (lead). **Carlos A. de Souza-Costa:** conceptualization (equal), formal analysis (equal), supervision (supporting), writing – review and editing (lead). **Paulo N. Lisboa-Filho:** conceptualization (equal), data curation (equal), supervision (equal), writing – review and editing (equal). **Diana G. Soares:** conceptualization (lead), data curation (lead), formal analysis (lead), funding acquisition (lead), investigation (supporting), methodology (supporting), project administration (lead), validation (supporting), visualization (lead), writing – original draft (supporting), writing – review and editing (lead).

Acknowledgments

The authors acknowledge the financial support received from the Coordenação de Aperfeiçoamento de Pessoal de Nível Superior—Brazil (CAPES)—Finance Code 001 and from the Fundação de Amparo à Pesquisa do Estado de São Paulo (FAPESP)—Grant Numbers 2016/15674-5 and 2022/05888-9. The Article Processing Charge for the publication of this research was funded by the Coordenação de Aperfeiçoamento de Pessoal de Nível Superior - Brasil (CAPES) (ROR identifier: 00x0ma614) [Correction added on May 14, 2025, after first online publication: CAPES funding statement has been added.]

Data Availability Statement

The data that support the findings of this study are available from the corresponding author upon reasonable request.

References

1. A. Banerjee, J. E. Frencken, F. Schwendicke, and N. P. T. Innes, "Contemporary Operative Caries Management: Consensus Recommendations on Minimally Invasive Caries Removal," *British Dental Journal* 223 (2017): 215–222.

2. H. F. Duncan, K. M. Galler, P. L. Tomson, et al., "European Society of Endodontology Position Statement: Management of Deep Caries and the Exposed Pulp," *International Endodontic Journal* 52 (2019): 923–934.

3. R. Islam, Y. Toida, F. Chen, et al., "Histological Evaluation of a Novel Phosphorylated Pullulan-Based Pulp Capping Material: An In Vivo Study on Rat Molars," *International Endodontic Journal* 54, no. 10 (2021): 1902–1914, https://doi.org/10.1111/iej.13587.

4. P. Sangwan, A. Sangwan, J. Duhan, and A. Rohilla, "Tertiary Dentinogenesis With Calcium Hydroxide: A Review of Proposed Mechanisms," *International Endodontic Journal* 46, no. 1 (2013): 3–19, https://doi.org/10.1111/j.1365-2591.2012.02101.x.

5. C. Dhand, S. T. Ong, N. Dwivedi, et al., "Bio-Inspired In Situ Crosslinking and Mineralization of Electrospun Collagen Scaffolds for Bone Tissue Engineering," *Biomaterials* 104 (2016): 323–338, https://doi.org/10.1016/j.biomaterials.2016.07.007.

6. D. G. Moussa and C. Aparicio, "Present and Future of Tissue Engineering Scaffolds for Dentin-Pulp Complex Regeneration," *Journal of Tissue Engineering and Regenerative Medicine* 13, no. 1 (2019): 58–75, https://doi.org/10.1002/term.2769.

7. D. G. Soares and V. Rosa, "Regenerating the Dental Pulp-Scaffold Materials and Approaches," *Dental Clinics of North America* 66, no. 4 (2022): 643–657, https://doi.org/10.1016/j.cden.2022.05.010.

8. Q. U. A. Malik, S. Iftikhar, S. Zahid, et al., "Smart Injectable Self-Setting Bioceramics for Dental Applications," *Materials Science & Engineering. C, Materials for Biological Applications* 113 (2020): 110956, https://doi.org/10.1016/j.msec.2020.110956.

9. N. Olov, S. Bagheri-Khoulenjani, and H. Mirzadeh, "Injectable Hydrogels for Bone and Cartilage Tissue Engineering: A Review," *Progress in Biomaterials* 11, no. 2 (2022): 113–135, https://doi.org/10.1007/s40204-022-00185-8.

10. L. Liu, D. Wu, H. Tu, et al., "Applications of Hydrogels in Drug Delivery for Oral and Maxillofacial Diseases," *Gels* 9, no. 2 (2023): 146, https://doi.org/10.3390/gels9020146.

11. B. J. Klotz, D. Gawlitta, A. J. Rosenberg, J. Malda, and F. P. Melchels, "Gelatin-Methacryloyl Hydrogels: Towards Biofabrication-Based Tissue Repair," *Trends in Biotechnology* 34, no. 5 (2016): 394–407, https://doi.org/10.1016/j.tibtech.2016.01.002.

12. Y. Liu and M. B. Chan-Park, "A Biomimetic Hydrogel Based on Methacrylated Dextran-Graft-Lysine and Gelatin for 3D Smooth Muscle Cell Culture," *Biomaterials* 31, no. 6 (2010): 1158–1170, https://doi.org/10.1016/j.biomaterials.2009.10.040.

13. N. Monteiro, G. Thrivikraman, A. Athirasala, et al., "Photopolymerization of Cell-Laden Gelatin Methacryloyl Hydrogels Using a Dental Curing Light for Regenerative Dentistry," *Dental Materials* 34, no. 3 (2018): 389–399, https://doi.org/10.1016/j.dental.2017.11.020.

14. E. A. F. Bordini, J. A. Ferreira, N. Dubey, et al., "Injectable Multifunctional Drug Delivery System for Hard Tissue Regeneration Under Inflammatory Microenvironments," *ACS Applied Bio Materials* 4, no. 9 (2021): 6993–7006, https://doi.org/10.1021/acsabm.1c00620.

15. I. S. P. da Silva, E. A. F. Bordini, E. S. Bronze-Uhle, et al., "Photo-Crosslinkable Hydrogel Incorporated With Bone Matrix Particles for Advancements in Dentin Tissue Engineering," *Journal of Biomedical Materials Research. Part A* 112, no. 12 (2024): 2273–2288, https://doi.org/10.1002/jbm.a.37777.

16. D. G. Soares, E. A. F. Bordini, W. B. Swanson, C. A. de Souza Costa, and M. C. Bottino, "Platform Technologies for Regenerative Endodontics From Multifunctional Biomaterials to Tooth-On-a-Chip Strategies," *Clinical Oral Investigations* 25, no. 8 (2021): 4749–4779, https://doi.org/10.1007/s00784-021-04013-4.

17. D. G. Soares, G. Anovazzi, E. A. F. Bordini, et al., "Biological Analysis of Simvastatin-Releasing Chitosan Scaffold as a Cell-Free System for Pulp-Dentin Regeneration," *Journal of Endodontics* 44, no. 6 (2018): 971–976, https://doi.org/10.1016/j.joen.2018.02.014.

18. D. G. Soares, Z. Zhang, F. Mohamed, T. W. Eyster, C. A. de Souza Costa, and P. X. Ma, "Simvastatin and Nanofibrous Poly(l-Lactic Acid) Scaffolds to Promote the Odontogenic Potential of Dental Pulp Cells in an Inflammatory Environment," *Acta Biomaterialia* 68 (2018): 190–203, https://doi.org/10.1016/j.actbio.2017.12.037.

19. D. G. Soares, E. A. F. Bordini, E. S. Bronze-Uhle, et al., "Chitosan-Calcium-Simvastatin Scaffold as an Inductive Cell-Free Platform," *Journal of Dental Research* 100, no. 10 (2021): 1118–1126, https://doi.org/10.1177/00220345211024207.

20. E. S. Bronze-Uhle, C. C. D. S. B. Melo, I. S. P. da Silva, et al., "Simvastatin-Loaded Chitosan Microspheres as a Biomaterial for Dentin Tissue Engineering," *Journal of Biomedical Materials Research. Part B, Applied Biomaterials* 113, no. 2 (2025): e35536, https://doi.org/10.1002/jbm.b.35536.

21. K. J. Rambhia and P. X. Ma, "Controlled Drug Release for Tissue Engineering," *Journal of Controlled Release* 219 (2015): 119–128, https://doi.org/10.1016/j.jconrel.2015.08.049.

22. Y. Jiang, N. Krishnan, J. Heo, R. H. Fang, and L. Zhang, "Nanoparticle-Hydrogel Superstructures for Biomedical Applications," *Journal of Controlled Release* 324 (2020): 505–521, https://doi.org/10.1016/j.jconrel.2020.05.041.

23. J. Long, A. E. Etxeberria, C. Kornelsen, et al., "Development of a Long-Term Drug Delivery System With Levonorgestrel-Loaded Chitosan Microspheres Embedded in Poly(Vinyl Alcohol) Hydrogel," *ACS Applied Bio Materials* 2, no. 7 (2019): 2766–2779, https://doi.org/10.1021/acsabm.9b00190.

24. R. Tanigo, Y. Takaoka, and J. Tabata, "Sustained Release of Water-Insoluble Simvastatin From Biodegradable Hydrogel Augments Bone Regeneration," *Journal of Controlled Release* 143 (2010): 201, https://doi.org/10.1016/j.jconrel.2009.12.027.

25. T. M. Faris, G. I. Harisa, F. K. Alanazi, A. M. Samy, and F. A. Nasr, "Developed Simvastatin Chitosan Nanoparticles Co-Crosslinked With Tripolyphosphate and Chondroitin Sulfate for ASGPR-Mediated Targeted HCC Delivery With Enhanced Oral Bioavailability," *Saudi Pharmaceutical Journal* 28, no. 12 (2020): 1851–1867, https://doi.org/10.1016/j.jsps.2020.11.012.

26. W. Gao, Y. Zhang, Q. Zhang, and L. Zhang, "Nanoparticle-Hydrogel: A Hybrid Biomaterial System for Localized Drug Delivery," *Annals of Biomedical Engineering* 44, no. 6 (2016): 2049–2061, https://doi.org/10.1007/s10439-016-1583-9.

27. S. Merino, C. Martín, K. Kostarelos, M. Prato, and E. Vázquez, "Nanocomposite Hydrogels: 3D Polymer-Nanoparticle Synergies for on-Demand Drug Delivery," *ACS Nano* 9, no. 5 (2015): 4686–4697, https://doi.org/10.1021/acsnano.5b01433.

28. M. Rezazadeh, M. Parandeh, V. Akbari, Z. Ebrahimi, and A. Taheri, "Incorporation of Rosuvastatin-Loaded Chitosan/Chondroitin Sulfate Nanoparticles Into a Thermosensitive Hydrogel for Bone Tissue Engineering: Preparation, Characterization, and Cellular Behavior," *Pharmaceutical Development and Technology* 24, no. 3 (2019): 357–367, https://doi.org/10.1080/10837450.2018.1484765.

29. A. Miyazawa, T. Matsuno, K. Asano, Y. Tabata, and T. Satoh, "Controlled Release of Simvastatin From Biodegradable Hydrogels Promotes Odontoblastic Differentiation," *Dental Materials Journal* 34, no. 4 (2015): 466–474, https://doi.org/10.4012/dmj.2014-272.

30. Y. Zhang, M. Chen, J. Tian, et al., "In Situ Bone Regeneration Enabled by a Biodegradable Hybrid Double-Network Hydrogel," *Biomaterials Science* 7, no. 8 (2019): 3266–3276, https://doi.org/10.1039/c9bm00561g.

31. Y. Li, C. Liu, W. Liu, et al., "Apatite Formation Induced by Chitosan/Gelatin Hydrogel Coating Anchored on Poly(Aryl Ether Nitrile Ketone) Substrates to Promote Osteoblastic Differentiation," *Macromolecular Bioscience* 21, no. 11 (2021): e2100262, https://doi.org/10.1002/mabi.202100262.

32. A. Moghimikheirabadi, M. Kröger, and A. V. Karatrantos, "Insights From Modeling Into Structure, Entanglements, and Dynamics in Attractive Polymer Nanocomposites," *Soft Matter* 17, no. 26 (2021): 6362–6373, https://doi.org/10.1039/d1sm00683e.

33. J. Liu, L. Li, H. Suo, M. Yan, J. Yin, and F. J. Fu, "3D Printing of Biomimetic Multi-Layered GelMA/nHA Scaffold for Osteochondral Defect Repair," *Maternal and Child Health Journal* 171 (2019): 107708, https://doi.org/10.1016/j.matdes.2019.107708.

34. M. Vigata, C. Meinert, S. Pahoff, N. Bock, and D. W. Hutmacher, "Gelatin Methacryloyl Hydrogels Control the Localized Delivery of Albumin-Bound Paclitaxel," *Polymers (Basel)* 12, no. 2 (2020): 501, https://doi.org/10.3390/polym12020501.

35. K. Elkhoury, L. Sanchez-Gonzalez, P. Lavrador, et al., "Gelatin Methacryloyl (GelMA) Nanocomposite Hydrogels Embedding Bioactive Naringin Liposomes," *Polymers (Basel)* 12, no. 12 (2020): 2944, https://doi.org/10.3390/polym12122944.

36. A. L. Frischknecht, E. S. McGarrity, and M. E. Mackay, "Expanded Chain Dimensions in Polymer Melts With Nanoparticle Fillers," *Journal of Chemical Physics* 132, no. 20 (2010): 204901, https://doi.org/10.1063/1.3428760.

37. J. Hao and R. A. Weiss, "Viscoelastic and Mechanical Behavior of Hydrophobically Modified Hydrogels," *Macromolecules* 44, no. 23 (2011): 9390–9398, https://doi.org/10.1021/ma202130u.

38. G. Miquelard-Garnier, S. Demoures, C. Creton, and D. Hourdet, "Synthesis and Rheological Behavior of New Hydrophobically Modified Hydrogels With Tunable Properties," *Macromolecules* 39 (2006): 8128–8139, https://doi.org/10.1021/ma061361n.

39. K. Rahali, G. Ben Messaoud, C. J. F. Kahn, et al., "Synthesis and Characterization of Nanofunctionalized Gelatin Methacrylate Hydrogels," *International Journal of Molecular Sciences* 18, no. 12 (2017): 2675, https://doi.org/10.3390/ijms18122675.

40. S. Chen, Y. Wang, J. Lai, S. Tan, and M. Wang, "Structure and Properties of Gelatin Methacryloyl (GelMA) Synthesized in Different Reaction Systems," *Biomacromolecules* 24, no. 6 (2023): 2928–2941, https://doi.org/10.1021/acs.biomac.3c00302.

41. R. Leu Alexa, H. Iovu, J. Ghitman, et al., "3D-Printed Gelatin Methacryloyl-Based Scaffolds With Potential Application in Tissue Engineering," *Polymers (Basel)* 13, no. 5 (2021): 727, https://doi.org/10.3390/polym13050727.

42. R. Cheng, R. Yan, H. Liu, et al., "Mechanically Enhanced Lipo-Hydrogel With Controlled Release of Multi-Type Drugs for Bone Regeneration," *Applied Materials Today* 12 (2018): 294, https://doi.org/10.1016/j.apmt.2018.06.008.

43. O. A. Monteiro, Jr. and C. Airoldi, "Some Studies of Crosslinking Chitosan-Glutaraldehyde Interaction in a Homogeneous System," *International Journal of Biological Macromolecules* 26, no. 2–3 (1999): 119–128, https://doi.org/10.1016/s0141-8130(99)00068-9.

44. W. Zeng, J. Huang, X. Hu, et al., "Ionically Cross-Linked Chitosan Microspheres for Controlled Release of Bioactive Nerve Growth Factor," *International Journal of Pharmaceutics* 421, no. 2 (2011): 283–290, https://doi.org/10.1016/j.ijpharm.2011.10.005.

45. Y. Xue, M. Wu, Z. Liu, et al., "In Vitro and In Vivo Evaluation of Chitosan Scaffolds Combined With Simvastatin-Loaded Nanoparticles for Guided Bone Regeneration," *Journal of Materials Science. Materials in Medicine* 30, no. 4 (2019): 47, https://doi.org/10.1007/s10856-019-6249-3.

46. K. Modaresifar, A. Hadjizadeh, and H. Niknejad, "Design and Fabrication of GelMA/Chitosan Nanoparticles Composite Hydrogel for Angiogenic Growth Factor Delivery," *Artificial Cells, Nanomedicine, and Biotechnology* 46, no. 8 (2018): 1799–1808, https://doi.org/10.1080/21691401.2017.1392970.

47. X. Zhao, Q. Lang, L. Yildirimer, et al., "Photocrosslinkable Gelatin Hydrogel for Epidermal Tissue Engineering," *Advanced Healthcare Materials* 5, no. 1 (2016): 108–118, https://doi.org/10.1002/adhm.201500005.

48. N. Celikkin, S. Mastrogiacomo, J. Jaroszewicz, X. F. Walboomers, and W. Swieszkowski, "Gelatin Methacrylate Scaffold for Bone Tissue Engineering: The Influence of Polymer Concentration," *Journal of Biomedical Materials Research. Part A* 106, no. 1 (2018): 201–209, https://doi.org/10.1002/jbm.a.36226.

49. J. W. Nichol, S. T. Koshy, H. Bae, C. M. Hwang, S. Yamanlar, and A. Khademhosseini, "Cell-Laden Microengineered Gelatin Methacrylate Hydrogels," *Biomaterials* 31, no. 21 (2010): 5536–5544, https://doi.org/10.1016/j.biomaterials.2010.03.064.

50. Y. C. Chen, R. Z. Lin, H. Qi, et al., "Functional Human Vascular Network Generated in Photocrosslinkable Gelatin Methacrylate Hydrogels," *Advanced Functional Materials* 22, no. 10 (2012): 2027–2039, https://doi.org/10.1002/adfm.201101662.

51. K. Yue, G. de Trujillo- Santiago, M. M. Alvarez, A. Tamayol, N. Annabi, and A. Khademhosseini, "Synthesis, Properties, and Biomedical Applications of Gelatin Methacryloyl (GelMA) Hydrogels," *Biomaterials* 73 (2015): 254–271, https://doi.org/10.1016/j.biomaterials.2015.08.045.

52. C. Dannert, B. T. Stokke, and R. S. Dias, "Nanoparticle-Hydrogel Composites: From Molecular Interactions to Macroscopic Behavior," *Polymers (Basel)* 11, no. 2 (2019): 275, https://doi.org/10.3390/polym11020275.

53. T. Hao and R. E. Riman, "Calculation of Interparticle Spacing in Colloidal Systems," *Journal of Colloid and Interface Science* 297, no. 1 (2006): 374–377, https://doi.org/10.1016/j.jcis.2004.10.014.

54. L. T. Yan and X. M. Xie, "Computational Modeling and Simulation of Nanoparticle Self-Assembly in Polymeric Systems: Structures, Properties and External Field Effects," *Progress in Polymer Science* 38 (2013): 369–405, https://doi.org/10.1016/j.progpolymsci.2012.05.001.

55. Y. Okamoto, W. Sonoyama, M. Ono, et al., "Simvastatin Induces the Odontogenic Differentiation of Human Dental Pulp Stem Cells In Vitro and In Vivo," *Journal of Endodontics* 35, no. 3 (2009): 367–372, https://doi.org/10.1016/j.joen.2008.11.024.

56. M. M. I. Sabandal, E. Schäfer, J. Aed, S. Jung, J. Kleinheinz, and S. Sielker, "Simvastatin Induces Adverse Effects on Proliferation and Mineralization of Human Primary Osteoblasts," *Head & Face Medicine* 16, no. 1 (2020): 18, https://doi.org/10.1186/s13005-020-00232-4.

57. M. M. I. Sabandal, E. Schäfer, J. Imper, S. Jung, J. Kleinheinz, and S. Sielker, "Simvastatin Induces in Vitro Mineralization Effects of Primary Human Odontoblast-Like Cells," *Materials (Basel)* 13, no. 20 (2020): 4679, https://doi.org/10.3390/ma13204679.

58. P. Rewthamrongsris, S. Phothichailert, U. Chokechanachaisakul, C. Kornsuthisopon, and T. Osathanon, "Simvastatin Induces Apoptosis but Attenuates Migration in SCAPs," *International Dental Journal* 74, no. 2 (2024): 352–358, https://doi.org/10.1016/j.identj.2023.10.015.

59. P. C. Chang, L. Y. Chong, A. S. Dovban, et al., "Sequential Platelet-Derived Growth Factor-Simvastatin Release Promotes Dentoalveolar Regeneration," *Tissue Engineering. Part A* 20, no. 1–2 (2014): 356–364, https://doi.org/10.1089/ten.TEA.2012.0687.

60. N. A. Aminabadi, B. Huang, M. Samiei, S. Agheli, Z. Jamali, and S. Shirazi, "A Randomized Trial Using 3Mixtatin Compared to MTA in Primary Molars With Inflammatory Root Resorption: A Novel Endodontic Biomaterial," *Journal of Clinical Pediatric Dentistry* 40, no. 2 (2016): 95–102, https://doi.org/10.17796/1053-4628-40.2.95.

61. Y. J. Chen and L. S. Chang, "Simvastatin Induces NFκB/p65 Down-Regulation and JNK1/c-Jun/ATF-2 Activation, Leading to Matrix Metalloproteinase-9 (MMP-9) but Not MMP-2 Down-Regulation in Human Leukemia Cells," *Biochemical Pharmacology* 92, no. 4 (2014): 530–543, https://doi.org/10.1016/j.bcp.2014.09.026.

62. M. B. Sordi, R. B. Curtarelli, I. F. Mantovani, et al., "Enhanced Osteoinductive Capacity of Poly(Lactic-Co-Glycolic) Acid and Biphasic Ceramic Scaffolds by Embedding Simvastatin," *Clinical Oral Investigations* 26, no. 3 (2022): 2693–2701, https://doi.org/10.1007/s00784-021-04240-9.

63. S. Kabra, N. R. Thosar, and N. S. Malviya, "Exploring the Synergistic Effect of Simvastatin in Oral Health Applications: A Literature Review," *Cureus* 15, no. 8 (2023): e44411, https://doi.org/10.7759/cureus.44411.

64. A. Ahmadi, R. Mazloomnejad, M. Kasravi, et al., "Recent Advances on Small Molecules in Osteogenic Differentiation of Stem Cells and the Underlying Signaling Pathways," *Stem Cell Research & Therapy* 13, no. 1 (2022): 518, https://doi.org/10.1186/s13287-022-03204-4.

65. M. M. Granat, J. Eifler-Zydel, and J. Kolmas, "Statins-Their Role in Bone Tissue Metabolism and Local Applications With Different Carriers," *International Journal of Molecular Sciences* 25, no. 4 (2024): 2378, https://doi.org/10.3390/ijms25042378.

66. M. S. Bae, D. H. Yang, J. B. Lee, et al., "Photo-Cured Hyaluronic Acid-Based Hydrogels Containing Simvastatin as a Bone Tissue Regeneration Scaffold," *Biomaterials* 32, no. 32 (2011): 8161–8171, https://doi.org/10.1016/j.biomaterials.2011.07.045.

67. Y. Naito, T. Terukina, S. Galli, et al., "The Effect of Simvastatin-Loaded Polymeric Microspheres in a Critical Size Bone Defect in the Rabbit Calvaria," *International Journal of Pharmaceutics* 461, no. 1–2 (2014): 157–162, https://doi.org/10.1016/j.ijpharm.2013.11.046.

68. O. Dianat, F. Mashhadiabbas, Z. Ahangari, S. Saedi, and S. R. Motamedian, "Histologic Comparison of Direct Pulp Capping of Rat Molars

With MTA and Different Concentrations of Simvastatin Gel," *Journal of Oral Science* 60, no. 1 (2018): 57–63, https://doi.org/10.2334/josnusd.16-0690.

69. K. Mahendran, C. Ponnusamy, and S. A. Maloor, "Histological Evaluation of Pulpal Response to Direct Pulp Capping Using Statins With α-Tricalcium Phosphate and Mineral Trioxide Aggregate in Human Teeth," *Journal of Conservative Dentistry* 22, no. 5 (2019): 441–448, https://doi.org/10.4103/JCD.JCD_418_19.

70. W. Jia, Y. Zhao, J. Yang, et al., "Simvastatin Promotes Dental Pulp Stem Cell-Induced Coronal Pulp Regeneration in Pulpotomized Teeth," *Journal of Endodontics* 42, no. 7 (2016): 1049–1054, https://doi.org/10.1016/j.joen.2016.03.007.

Supporting Information

Additional supporting information can be found online in the Supporting Information section.